Development of GFRP-Reinforced Concrete Bridge Barrier-Deck Slab Details to Resist Equivalent Vehicle Impact Loading

H.R Khederzadeh[1] and K. Sennah[1]
[1]Civil Engineering Department, Ryerson University, Toronto, Ontario, Canada M5B 2K3

ABSTRACT: Corrosion of steel reinforcement due to environmental effects is a major cause of deterioration problems in bridge barriers. Glass fibre reinforced polymers (GFRP) not only addresses this durability problem but also provides exceptionally high tensile strength. A recent design work conducted at Ryerson University on PL-3 bridge barrier has led to an economical GFRP bar detailing for sustainable construction. The special sand-coated GFRP bars and end anchorage heads ensure optimal bond between concrete and the bar and eliminate the use of custom-made and costly bar bends. In this paper, three configuration of GFRP detailing for PL-3 barriers were proposed based on the available AASHTO-LRFD yield-line failure equation and the CHBDC factored applied moment at the barrier-deck junction. Five full-scale barrier models of 1000 mm length, representing PL-3 barriers were erected and tested to-collapse to determine their ultimate load carrying capacities and failure modes. Four barriers were erected using GFRP bars. Two of which were built using high-modulus (HM) GFRP bars with end anchorage heads, while the other two were built using GFRP bent and 180˚ hook, respectively, with standard-modulus (SM) V-Rod bars. Barrier five, as a reference barrier mode, was made of conventional steel reinforcements as per MTO barrier drawings. This paper presents the results from these tests in the form of crack pattern, deflection history and the ultimate load carrying capacity as compared to the design values specified in the Canadian Highway Bridge Design Code (CHBDC) for barrier anchorage into the deck slabs. It was observed that the experimental ultimate load carrying capacities of the barriers were observed to be greater than the CHBDC factored design loads.

1. INTRODUCTION

Conventional Bridges built prior to the 1970's did not use air-entrained concrete and coated reinforcing steel bars to protect from the effects of freeze-thaw cycles and the application of winter de-icing salt. This leads to corrosion-induced degradation in bridge elements as shown in Fig. 1. Accordingly, exposed bridge elements are all likely candidates for expensive replacement on the majority of these older bridges. In November 2007, The Residential and Civil Construction Alliance of Ontario, Canada, (RCCAO 2007) released a report on the state of Ontario bridges, entitled "Ontario's Bridges: Bridging the Gap." The report warns that the integrity of Ontario's municipal bridge infrastructure and public safety are at risk after years of deferred maintenance, irregular inspections, and lack of government oversight. The RCCAO report stated some recommendations to be made to promote the public's safety and the sustainability of Ontario's bridges. One of these recommendations includes promoting bridge engineering designs that improve the life expectancy and reduce maintenance costs of bridges. This can be achieved by using fibre reinforced polymer bars.

Fibre-reinforced polymers (FRPs), as non-corrodible materials, are considered as excellent alternative to reinforcing steel bars in bridge decks to overcome steel corrosion-related problems. Since it is less expensive than carbon and aramid FRPs, Glass FRP (GFRP) bars are more attractive to bridge deck and barrier applications. Two types of GFRP bars were considered in used in this study, namely: (i) GFRP bars with high modulus (HM) and (ii) GFRP bars with standard modulus (SM). The sand-coated surface profile of these bars, shown in Fig. 2, ensure optimal bond between concrete and the bar. Table 1 summarizes the material

properties of the bars considered in this study (Pultrall, 2012). It should be noted that the bent bars and bars with 180° hook are manufactured using standard modulus material. The modulus of elasticity of such bent bars is determined to be 50 MPa and the tensile strength of the bar at the bent of hook locations is considered 473 MPa in this study.

Fig.1 Corrosion-induced degradation of steel-reinforced bridge barrier wall

Fig. 2 View of GFRP bars types

Table 1 GFRP material Properties

Product type	Bar size	Diameter (mm)	Cross-section area (mm^2)	Guaranteed tensile strength (MPa)	Modulus of elasticity (MPa)	Strain at failure
High modulus (HM)	#4 (12M)	12.70	126.7	1312	65.6±2.5	2.0%
	#5 (15M)	15.88	197.9	1184	62.5±2.5	1.89%
	#6 (20M)	19.05	285.0	1105	64.7±2.5	1.70%
Standard modulus (SM)	#4 (12M)	12.70	126.7	941	53.60±2.5	1.76%
	#5 (15M)	15.88	197.9	934	55.40±2.5	1.69%
	#6 (20M)	19.05	285.0	807	56.60±2.5	1.43%
SM-bent	#5 (15M)	15.88	197.9	473 (bent portion) 1051 (straight portion)	50	1%
SM-180° hook	#5 (15M)	15.88	197.9	473 (bent portion) 1051 (straight portion)	50	1%

3. BACKGROUND OF THE DEVELOPED GFRP-REINFORCED BARRIER

The design process of bridge barrier walls is specified in the Canadian Highway Bridge Design Code (CSA, 2006a; CSA, 2006b) for both the barrier wall and the barrier-deck slab joint. CHBDC Clause 12.4.3.5 specifies that the suitability of a traffic barrier anchorage to the deck slab shall be based on its performance during crash testing of the traffic barrier. For an anchorage to be considered acceptable, significant damage shall not occur in the anchorage or deck during crash testing. It also specifies that if crash testing results for the anchorage are not available, the anchorage and deck shall be designed to resist the maximum bending, shear and punching loads that can be transmitted to them by the barrier wall. As such, the initial design of the proposed PL-3 precast bridge barrier (Sennah et al., 2010) was carried out to meet the CHBDC design criteria specified for static loading at the anchorage between the deck slab and the barrier wall. CHBDC specifies transverse, longitudinal and vertical loads of 210, 70 and 90 kN, respectively, that can be applied simultaneously over a certain barrier length. CHBDC specifies that transverse load shall be applied over a barrier length of 2400 mm for PL-3 barriers. Since transverse loading creates the critical load carrying capacity, both the longitudinal and vertical loads were not considered in the design of barrier wall reinforcement and anchorages between the deck slab and the barrier wall. It should be noted that CHDBC specifies a live load factor of 1.7. Thus, the design impact load on PL-3 barrier wall over 2.4 m length is 357 kN. As for the design of the vertical and horizontal reinforcement in the barrier wall, AASHTO-LRFD Bridge Design Specifications (AASHTO, 2010) specify the yield-line analysis for the ultimate flexural capacity of the barrier wall. However, such failure more is not applicable to GFRP-reinforced barrier wall

due to the difference in the modulus of elasticity between steel and GFRP bars. As such, proposed GFRP-reinforced barrier-deck detailing has to be examined by experimental testing.

Most recently, a preliminary design work conducted at Ryerson University for the PL-3 bridge barrier led to the second world-wide vehicle crash test recently conducted by Ryerson University research team (Sennah and Kederzadeh, 2012) on GFRP-reinforced PL-3 barrier. In the crash-tested barrier, as shown in Fig. 3a, 15M and 12M GFRP bars were used as vertical reinforcement in the barrier front and back face, respectively, with 12M GFRP bars as horizontal reinforcement, all at 300 mm spacing. The connection between the deck slab and the barrier wall utilized the GFRP headed end bars for proper anchorage. It should be noted that this new arrangement of the GFRP bars would significantly reduce the cost, given the increased spacing of the vertical bars to 300 mm. Also, the traditional lap splice of the vertical bars at the back face of the barrier wall as well as the bents of these bars in the bridge deck slab, shown in Fig. 3b, were eliminated to reduce the material and labor cost. This decision was reached due the fact that the vertical bars at the back face of the barrier walls are always in compression when the barrier is subjected to vehicle impact.

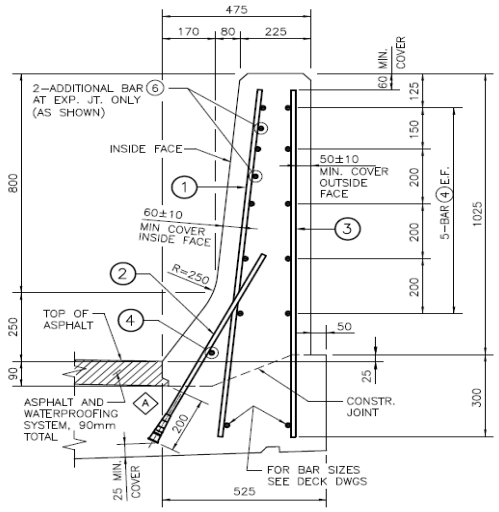

Fig. 3a Barrier detailing from MTO Standard Drawing SS110-92 (MTO, May 2011)

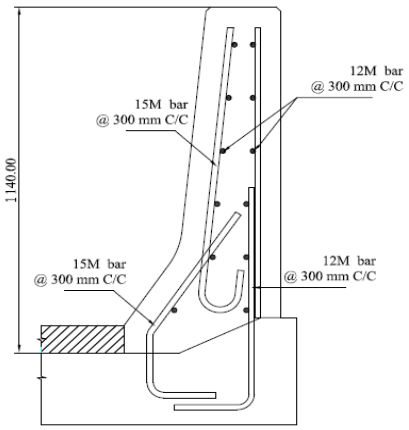

Fig. 3b Traditional barrier reinforcement with bent bars

Given the fact that the material cost of the GFRP bars differs based on the type of the bar (i.e. high-modulus versus standard modulus, straight bars versus bent bars and headed-end bars versus bars with 180° hooks), Ryerson University research team developed three different GFRP bar detailing as shown in Fig. 4. Proposal No. 1 in this figure incorporated HM bars with headed ends embedded in the deck slab that was successfully crashed-tested as mentioned earlier. While proposal No.2 incorporated SM bars with bents. Proposal No. 3 incorporated SM bars with 180° hooks embedded in the deck slab. It should be noted that Ryerson University research team has built and tested to collapse full-scale barrier segments of 1 m length to determine their anchorage capacity with the deck slab cantilever. Based on the results from these tests and cost estimates of GFRP material content, other crash test will be conducted on either proposal No. 2 or 3 to qualify it for use in Canada's bridges.

4. EXPERIMENTAL STUDY ON PL-3 BARRIER MODELS

Five full-scale PL-3 barrier models were erected and tested to-collapse to determine their ultimate load carrying capacities and failure modes. The length of the barriers was taken 900 mm for barrier models 1 and 2 and 1000 mm for barrier models of 3, 4 and 5 to investigate the barrier-deck anchorage strength. Concrete cover to front and back GFRP bars in the barrier walls and top layer of the bars in the deck slab was taken as 50 mm. The PL-3 barrier walls had a thickness of 225 mm from top surface, which is proportionally increased to 305mm at a depth of 800 mm and tapered to 475 mm at depth of 1025 to the deck slab-barrier joint. The concrete deck slab had an average thickness of 300 mm under the barrier wall which is reduced to 250 mm in the slab portion, and reinforced with M20 Steel bars at the top reinforcement

layer with 100 mm spacing and M15 Steel bars at 300 mm spacing at the bottom reinforcement layer in the direction normal and parallel to the wall, respectively. In barrier models 1 to 4, sand-coated GFRP bars were used as vertical and horizontal reinforcement in front and back face of the barrier, while the fifth barrier was constructed using reinforcing steel bars only as a reference specimen. All barriers were casted using 25.4 MPa concrete.

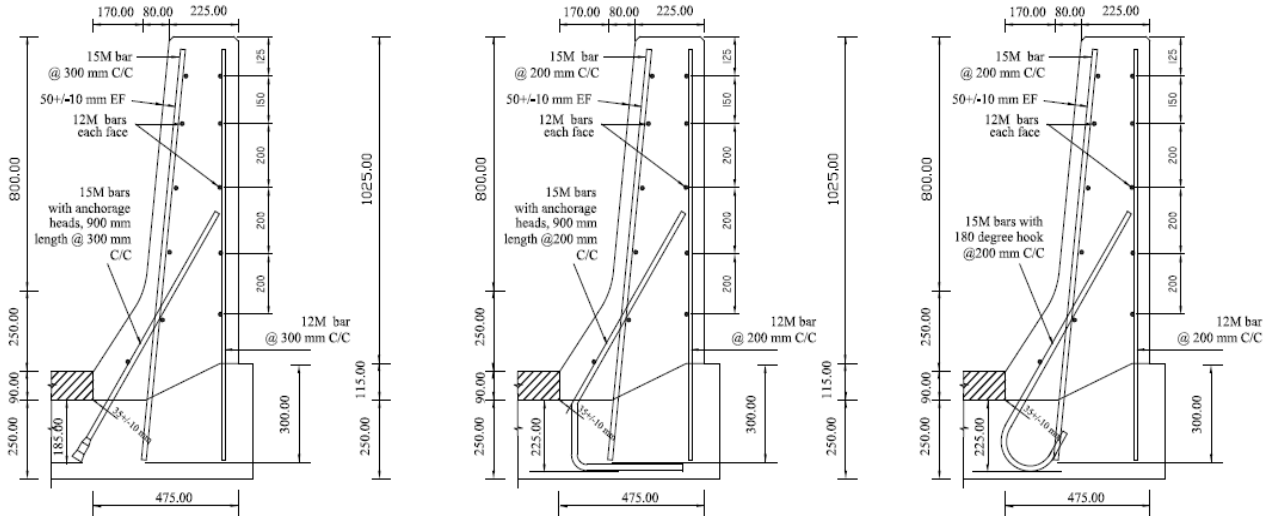

a) Proposal No. 1 (b) Proposal No. 2 c) Proposal No. 3

Fig. 4 Proposed Ryerson University GFRP-Reinforced Barrier Details

Model 1 was constructed using High-Modulus (HM) GFRP bars as shown in Fig. 4(a). 15M HM-GFRP bars with head end were placed at 300 mm c/c spacing in front face of the barrier at deck-barrier joint. In addition, 15M HM-GFRP bars were placed in the front face of the barrier wall extending into the deck slab at 300 mm spacing. 12M HM-GFRP bars were placed as horizontal reinforcement as well as vertical reinforcement in back face of the wall at 300 mm spacing. Figure 5 shows view of GFRP bar arrangement in Model 1. Model 2 incorporated Standard Modulus (SM) GFRP bars in the barrier wall as depicted in Fig. 4(2). At the junction of barrier to the deck slab, M15 GFRP bent bars were placed at 200 mm spacing in the barrier front face. In addition, M15 GFRP bars were placed at 200 mm spacing in the top tapered portion of the front face of the barrier, with the bars extended into the deck slab as shown in Fig. 4(2). M12 GFRP bars at 200 mm spacing were used as horizontal bars as well as vertical bars in back face of the barrier wall. Figure 6 shows view of GFRP bars in Model 2 before concrete casting.

Table 1 Barrier Designations used in this study for each model

Barrier Designation	Description of Models
GS1- HM	Specimen No.1 with GFRP bars and High Modulus of Elasticity -Headed-end bars with 300mm spacing
GS2- ST	Specimen No.2 with GFRP bars and Standard Modulus of Elasticity -90˚ bent bars with 200mm spacing
GS3- ST	Specimen No.3 with GFRP bars and Standard Modulus of Elasticity- 180˚ hook bars with 200mm spacing
GS4- HM	Specimen No.4 with GFRP bars and High Modulus of Elasticity - Headed-end bars with 150mm spacing
SS5- CS	Specimen No.5 with Conventional Steel Reinforcement and 200mm bar spacing

Similar to barrier model 2, barrier model 3 was built using SM GFRP bars but with 180˚ hook at the junction of deck slab to the barrier wall. The SM GFRP bars placed on other locations in this model were identical to model 3. Figure 7 shows view of the placement of GFRP of bars in the formwork. Model 4 was constructed similar to model 1 except that the HM GFRP vertical bars were placed at 150 mm center-to-center spacing representing the barrier wall at its ends or at the construction joint locations. However, the spacing for GFRP horizontal bars as well as vertical bars in the back face of the wall was kept as 300 mm. Figure 8

shows a view of formwork with GFRP installation prior to concrete casting. Model 5 was constructed as reference sample using conventional steel reinforcement, as per MTO standard drawings for reinforced steel bridge barriers. Figure 9 shows a photo of this barrier model with steel reinforcement in front and back face of the wall as vertical and horizontal reinforcements. The M15 steel bar with 180° hook was placed to reinforce the top tapered portion of the barrier front face, while M15 bent bars were placed on the bottom tapered portion, all at 200 mm center-to-center spacing. M12 steel bars were placed in the model as horizontal bars as well as vertical bars in back face of the wall at 300 mm spacing. Table 2 summarises barrier configurations considered for testing in this study.

Figure 10 shows a schematic diagram of the test setup and the location of LVDT's. Each barrier specimen was supported over the structures laboratory floor, then, tied down to the floor using 50-mm diameter threaded rods. Each rod was placed @ 600 mm c-c and tightened by applying a specified torque to control the slab uplift during testing. A 900- kN hydraulic jack was used to apply horizontal load to the barrier wall. A universal flat load cell of 900-kN capacity was used to measure the applied loads on barrier models. SYSTEM 6000 data acquisition unit was used to record readings from all sensors. Each specimen was tested under increasing monotonic load up-to-collapse. During the test, jacking load was applied in increments of 10 kN. At each load increment, the load was maintained for a few minutes to observe crack initiation and propagation as well as change in barrier geometry as depicted from LVDT readings. Failure of the model was attained when the readings from sensors were increasing while the model did not take any further increase in load. Figure 10 shows LVDT's locations which were (i) at the top of the back side of the barrier wall oriented in the direction of the applied load; (ii) at the bottom of the deck slab to measure slab movement under transverse load; (iii) at the top of the back side of the deck slab to measure any possible uplift under load; and (iv) at back side of the wall to capture the possible vertical displacement of the barrier wall.

Fig. 5 View of GFRP bars in Model 1

Fig. 6 View of GFRP bars in Model 2

Fig. 7 View of barrier model 3

Fig. 8 View of barrier model 4

Fig. 9 View of barrier model 5

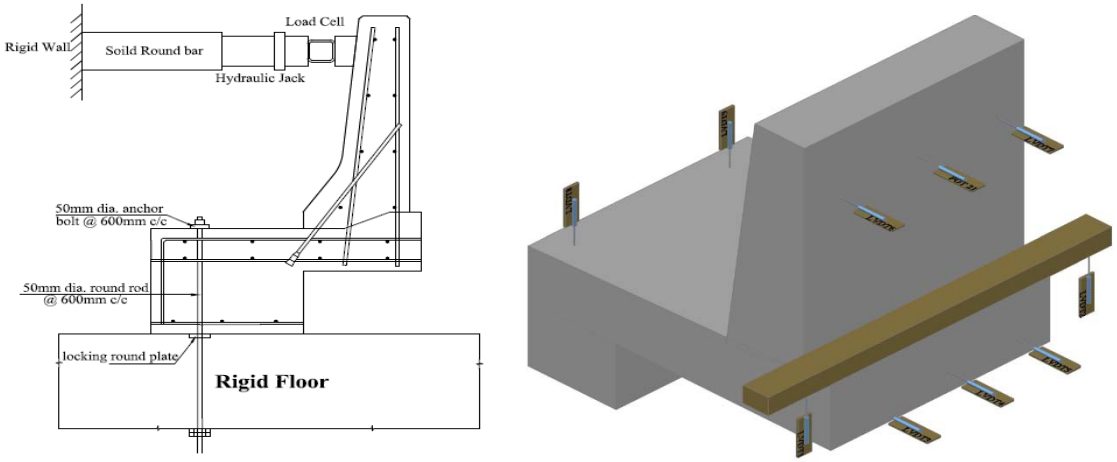

Fig. 10 Schematic diagram of test setup (left) and locations of LVDT's (right)

Table 3: Transverse moments in cantilever slabs due to horizontal railing loads in selected PL-3 and PL-2 barriers. (Table C5.4 in CHBDC Commentary, CSA 2006b)

Horizontal load or moment dispersion at inner portion of deck	**Performance Level 3 barrier**	**Performance Level 2 barrier with rail**
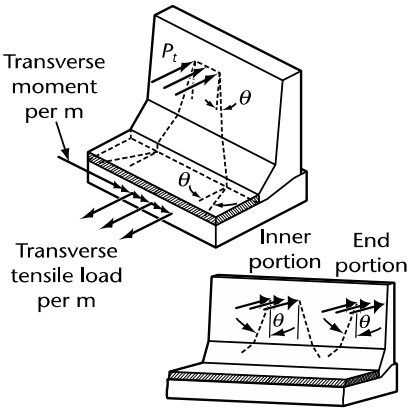	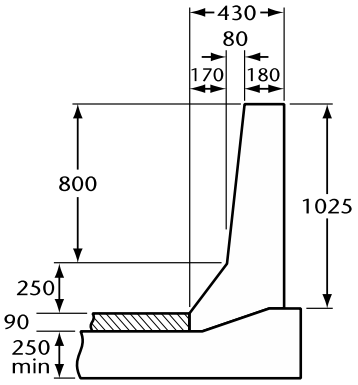	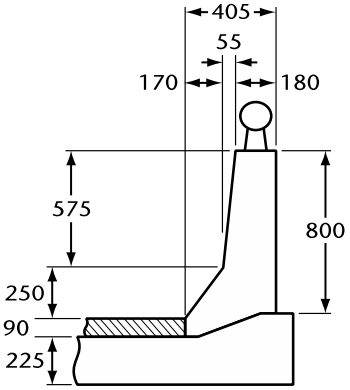
Factored horizontal load P_t (Clause 3.8.8.1)	357 kN	170 kN
Length of load application (Clause 12.5.2.4)	2400 mm	1050 mm
Height of load application above deck (Clause 12.5.2.4)	900 mm	700 mm
Moment in inner portions of deck per metre at face of barrier	83 kN-m/m	38 kN-m/m
Moment in end portion of deck per metre at face of barrier	102 kN-m/m	52 kN-m/m

5. TREANSVERSE MOEMENT IN CANTILIVER SLAB IN ACCORDANCE WITH CHBDC

CHBDC prescribes guidelines for the railing loads to be considered for the design of barrier anchorage and the edge of the deck slab in the bridge cantilever barriers. According to the maximum lateral loads and dispersion angle of the load effects along the height of the barrier (see Table 3), factored applied moments at the barrier-deck junction are given in CHBDC driven from Finite-Element (FE) Analysis. These are the resulting moments at the face of the barrier-to-deck joint used in the design of the barrier anchorage. Lateral load also exerts shear at the barrier anchorage which usually does not govern. CHBDC specifies

that the design of the barrier-deck anchorage capacity can be achieved by code-approved manual calculations or experimental testing under static loads to failure in lieu of conducting vehicle crash testing. The following section discusses the experimental findings and their correlation with CHBDC design values shown in Table 3.

6. EXPERIMENTAL RESULTS FOR THE TESTED PL-3 BARRIER MODELS

Figure 11 depicts view of the test setup for the tested barrier walls. As mentioned earlier, the barriers had concrete strength of 25.4 MPa. Barrier model 1 with HM- GFRP bars of headed end spaced at 300 mm c/c was tested to-complete-collapse. It should be noted that the length of this barrier was 900 mm in longitudinal direction. The load was applied at 990 mm above the deck slab per CHBDC for PL-3 barriers tested under static test. The load was applied manually using hydraulic jack and load increments were captured by load cell attached to the system. The load was applied in increments of 10 kN to observe the crack initiation in the barrier wall and the slab. The first visible flexural crack appeared at the junction of barrier wall-to-deck slab at load of 20 kN as depicted in Figs. 12 and 13. With load increase, cracks were further developed at the corner of deck-to-slab junction down into the deck slab. Similarly, cracks were initiated in the deck slab at 25 to 30 kN due to combined flexure and tension. At a load of 40 kN, flexural crack was observed at the junction of the upper and lower portions of the tapered wall. At this loading stage, cracks started to propagate horizontally through the thickness at the intersection of deck-to-barrier in addition to the cracks observed earlier in the slab. The cracks propagated significantly till the barrier reached the failure load of 95.49 kN. The barrier primary failure took place at the corner of deck-to-slab interface due to flexural mode of failure. As such, the ultimate moment resisted per meter length of the barrier wall was 95.49 kN x0.99 m height /0.9 m width = 105.04 kN.m/m which is greater than the CHBDC factored design moment of 83 kN.m/m shown in Table 2 for interior locations of the barrier wall. At failure stage, the average ultimate lateral deflection of barrier wall was recorded as 41.61 mm, while the deck slab showed an average horizontal movement of 1.63 mm. At failure, an average deck uplift of 2.87 mm was observed. Figure 14 shows load-deformation curves recorded for model 1.

Fig. 11 View of the barriers test setup

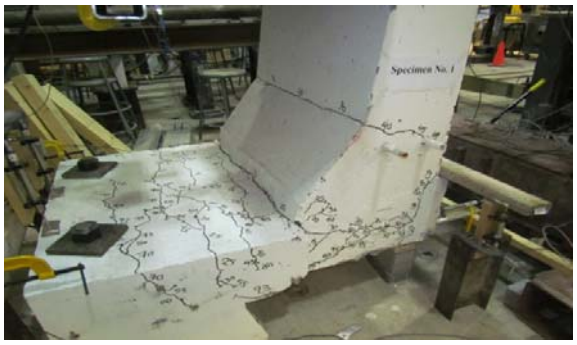

Fig. 12 View of the crack pattern in barrier model 1 with HM-GFRP bars at 300-mm spacing (right side)

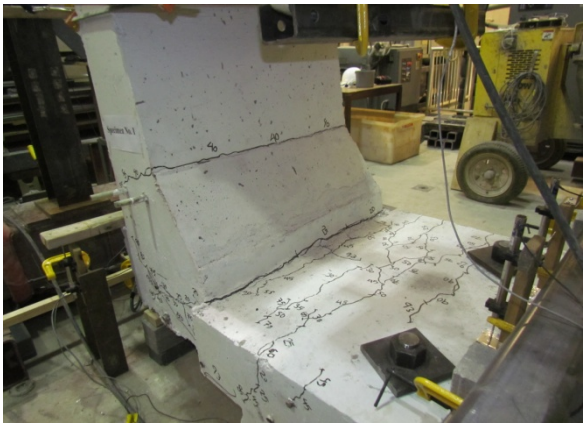

Fig. 13 View of the crack pattern in barrier model 1 with HM-GFRP bars at 300-mm spacing (left side)

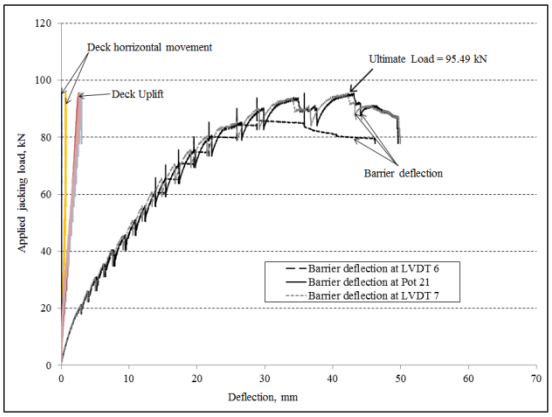

Fig. 14 Load-deformation curves of the barrier wall, deck movement and deck uplift of barrier model 1

In barrier model 2, Standard Modulus GFRP bent bars were placed vertically in the front face of the barrier wall at 200 mm spacing. The barrier had a length of 1000 mm in the longitudinal direction. The load was applied at 990 mm above the deck slab similar to barrier model 1. Figure 15 shows view of the crack pattern at failure. In this barrier model, the first flexural crack was observed at the fixed end of the deck slab at load of 40 kN. By increasing the load to 50 kN, cracks were further developed in the deck slab and vertical cracks appeared on each side of the deck slab due to combined tension and flexure loading. At 60 kN load, horizontal flexural crack was observed at the deck-to-barrier junction. A similar flexural crack was initiated at junction of the upper and lower portion of the tapered wall at load increment of 65 kN which was further developed into the wall thickness at higher load. At the load range of 70 to 100 kN, cracks propagated further into the slab and barrier thicknesses. At 100 kN load, a flexural crack was observed in the top tapered portion of the barrier wall. With increase in applied load, cracks propagated further into the deck thickness at the barrier-deck junction that led to failure at 116.32 kN primarily due to flexural crack barrier-deck region. As such, the maximum moment reached at failure of deck-to-barrier junction was 116.32 kN x 0.99 m = 115.2 kN.m/m. This ultimate load carrying capacity was greater than the factored design moment of 83 kN.m/m specified in CHBDC at interior location as shown in Table 2. The barrier wall exhibited an average lateral deformation of 46.43 mm with deck horizontal movement of 4.37 mm and deck uplift of 5.3 mm at failure. The load-deformation curves captured by LVDT's are displayed in Fig. 16.

Fig. 15 View of the crack pattern in barrier model 2 with SM-GFRP bent bars at 200 mm spacing

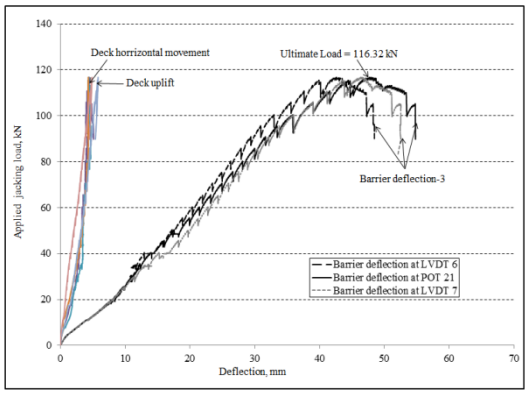

Fig. 16 Load-deformation curve of the barrier wall, deck movement and deck uplift of barrier model 2

Barrier model 3 was constructed using Standard Modulus GFRP bars by placing GFRP bars with 180˚ hooks at 200 mm spacing as vertical bars at front face of the barrier wall. It is worth to mention the barrier has a length of 1000 mm in the longitudinal direction. Similar to barrier model 1 and 2, the load was applied at 990 mm above the deck. Figure 17 shows view of the crack pattern at failure of model 3. The first visible flexural crack was observed at deck-barrier junction at an applied load of 30 kN. At this load, other flexural crack was also observed at junction of the top and bottom tapered portions of the barrier wall as well as in the deck slab. With increase in applied load to 45 kN, cracks started to propagate into the barrier-deck corner down into the slab thickness. Also, vertical cracks were detected in the deck slab when the load increased from 50 to 70 kN due combined tension and flexural loading on the deck slab. At this loading stage, cracks were further developed in corner junction of barrier-to-deck as well as through thickness in both the barrier wall and the deck slab. At 100 kN, a second flexural crack was observed in the top tapered portion of the barrier wall, extending significantly through thickness at the same load increment. Moreover, several flexural cracks were formed on the top surface of the deck slab at load ranging from 50 to 100 kN. Consequently, the barrier failed at load of 107.13 KN at the corner of barrier-to-deck junction due to combined tension and flexure in the deck slab. The resulting maximum moment at the barrier-deck junction was calculated as 107.13 kN x .99 m = 106.06 kN.m/m which is far greater that the CHBDC factored design moment of 83 kN.m/m for barrier tested at interior location. It should be noted that at failure, the barrier had an average deflection of 36.26 mm, with deck slab movement of 1.57 mm in horizontal direction and deck slab uplift of 4.24 mm. Figure 18 shows load-deformation curves of the barrier and deck slab under load.

In barrier model 4, the vertical High-Modulus GFRP bars were placed at 150 mm spacing in the front face of the barrier wall. Similar to other barriers, the load was applied 990 mm above the deck. Figure 19 shows view of the crack pattern of model 4 at failure. The first visible flexural crack was observed at the barrier-

deck joint at a load of 25 kN. Further cracks due to combined flexural and tension appeared in the deck slab with further increase in applied load. At 60 kN, flexural crack was observed at the junction of the top and bottom tapered portion of the barrier wall. At 70 kN load, a similar flexural crack was observed right above the junction between the top and bottom tapered portion of the wall and propagated significantly through the thickness at the same load increment. At this load increment, cracks were also propagated through thickness at the corner of the barrier-to-deck junction. At 95 kN load, a second flexural crack was observed in the top tapered portion of the wall barrier-deck corner, leading to barrier failure at 153.3 kN. The failure of the barrier occurred at lower portion of the deck slab due to concrete splitting at the compression side of the slab under the barrier wall. The experimental results led to a maximum applied moment at the barrier-deck junction of 153.32 kN x 0.99 m / 0.9 m = 168.6 kN.m/m which is far greater that the CHBDC factored design moment of 102 kN.m/m at barrier end location as shown in Table 3. It should be noted that the average lateral deformation of the barrier wall was 50.13 mm, with 5.53-mm average deck horizontal movement and 2.47-mm average deck uplift at failure ad depicted in Fig. 20 for model 4.

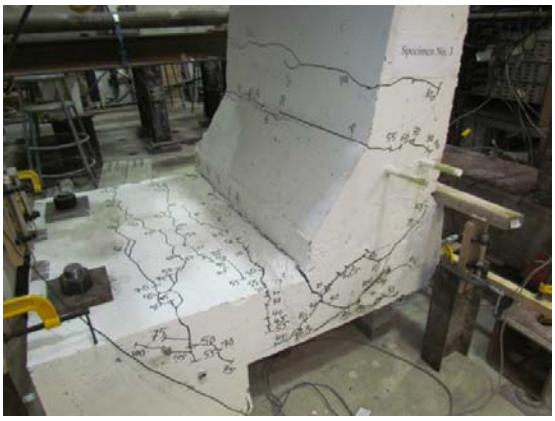

Fig. 17 View of the crack pattern in model 3 with SM-GFRP bars with 180° hooks at 200 mm spacing

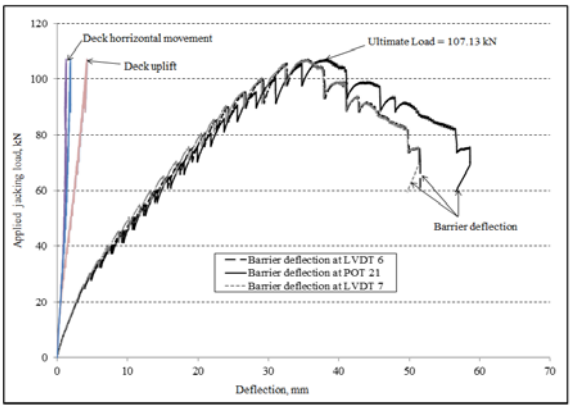

Fig. 18 Load-deformation curve of the barrier wall, deck movement and deck uplift of barrier model 3

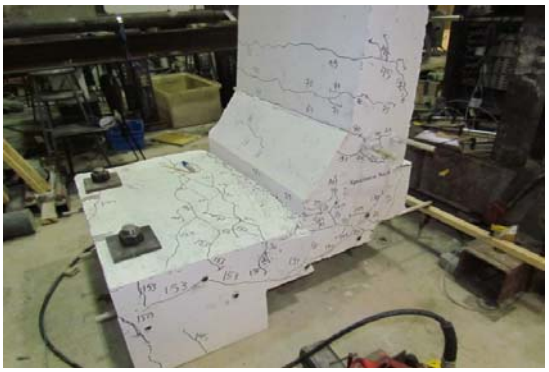

Fig. 19 View of the crack pattern in barrier model 4 with HM-GFRP bars at 150 mm spacing

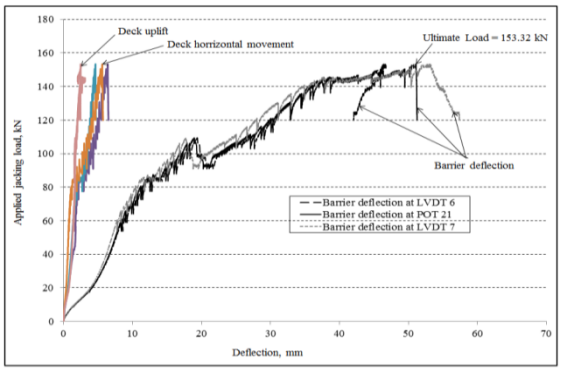

Fig. 20 Load-deformation curves of the barrier wall, deck movement and deck uplift of model 4

Barrier model 5 was constructed as reference model to compare the results with barrier models reinforced with GFRP bars. In this model, M15 steel bars were placed vertically in front face of the barrier wall at 200 mm spacing. Similar to GFRP-reinforced models, the load was applied at 990 mm above the deck slab. Figure 21 shows view of the crack pattern observed in barrier model 5 at failure. At load step of 20kN, the first visible flexural crack was observed at the barrier-to-deck junction, which was extended down into the slab at the corner of deck-barrier joint. With load increase to 50 kN, few flexural cracks were observed in the deck slab extending through the deck thickness. In addition, at load step of 50 kN, a flexural crack was developed at junction of the top and bottom tapered portion of the wall, which was extended into the wall thickness with load increase. With increase in load to 85 kN, few cracks were developed horizontally at the corner of the deck-barrier wall. With increase in the load to 105 kN, other flexural crack was observed in top portion of the tapered wall and propagated through the wall thickness with load increase. In addition, more

flexural cracks appeared at the top surface of the deck slab. With further increase in load, cracks widened, leading to barrier failure at 128.92 kN at corner junction of deck-to-barrier wall under combined tension and flexure. Results led to a maximum moment at the barrier-deck junction of 128.92 kN x 0.99 m = 127.63 kN.m/m which is far greater that the CHBDC factored design moment of 83 kN.m/m at interior location. The barrier wall displayed an average 32.81- mm maximum lateral deflection, with 5.03-mm deck slab horizontal movement and 2.67-mm deck uplift at failure as depicted in Fig. 22 for model 5.

Fig. 21 View of the crack pattern in barrier model 5 with steel bars at 200 mm spacing

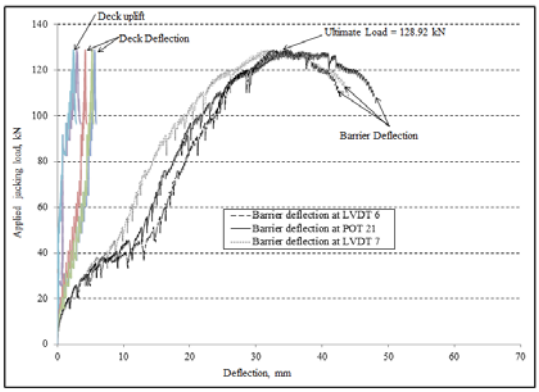

Fig. 22 Load-deformation curve of the barrier wall, deck movement and deck uplift of barrier model 5

7. CONCLUSION

Based on the data generated from the experimental study, it can be concluded that the proposed barrier reinforcement details incorporating GFRP bars with headed anchorage, GFRP bents and GFRP bars with 180˚ hook can be safely used in bridge barrier walls to resist the applied vehicle impact load specified in the Canadian Highway Bridge Design Code at the barrier wall-deck slab anchorage. Experimental findings showed that the proposed GFRP-reinforced barriers are as good as reinforced steel barrier with respect to strength at the barrier-deck junction. In addition, the maximum barrier deflection exhibited in the proposed GFRP-reinforced barriers is less than that observed for steel-reinforced barrier as attributed to the low flexural modulus of elasticity of the GFRP bars. Such increase in deflection would have a favorable effect in absorbing energy resulting from vehicle impact.

ACKNOWLEDGEMENTS

The authors acknowledge the research support by Pultrall Inc. Quebec, and Trancels-Pultrall Inc of Barrie, Ontario.

REFERENCES

AASHTO. 2010. *AASHTO-LRFD Bridge Design Specifications*. Third Edition, American Association of State Highway and Transportation Officials, Washington, DC.

CSA. 2006a. *Canadian Highway Bridge Design Code. CAN/CSA-S6-06*. Canadian Standard Association, Toronto, Ontario, Canada.

CSA. 2006b. *Commentary on CAN/CSA-S6-06, Canadian Highway Bridge Design Code*. Canadian Standard Association, Toronto, Ontario, Canada.

RCCAO. 2007. *Ontario's Bridges Bridging the Gap*. Report prepared by MMM Group for Residential and Construction Alliance of Ontario, RCCAO, 56 pages.

Pultrall Inc., Canada. 2012. www.pultrall.com.

Sennah, K., Tropynina, E., Goremykin, S., Lam, M., and Lucic, S. 2010. Concrete Bridge Barriers Reinforced with GFRP Bars with Headed Ends. Proceedings of the 8th International Conference on Short and Medium Span Bridges, Niagara Falls, Ontario, pp. 1-10.

Sennah, K and Kederzadeh, H. 2012. Vehicle Crash Testing of a PL-3 Concrete Bridge Barrier Reinforced with GFRP Bars with Sand-Coated Surface and Headed Ends. Technical Report submitted to Pultrall Inc. and Ontario Ministry of Transportation, 86 pages.